A Fe(II) Coordination Polymer Based on 1,10-Phenanthroline Derivative and Oxalic Acid: Synthesis, Structure, and Properties①

LI Xiu-Ying[a, b] GAO Lin[c] CHE Guang-Bo[b②]
YAN Yong-Sheng[a] LI Chun-Xiang[a②]

[a] (*School of Chemistry and Chemical Engineering, Jiangsu University, Zhenjiang* 212013, *China*)

[b] (*College of Chemistry, Jilin Normal University, Siping* 136000, *China*)

[c] (*College of Environmental Engineering, Jilin Normal University, Siping* 136000, *China*)

ABSTRACT A Fe-based coordination polymer, $[Fe(C_2O_4)_{0.5}(4\text{-NCP})]_n \cdot 2nH_2O$ (**1**, 4-HNCP = 2-(4-carboxy-phenyl)-1H-imidazo(4,5-f)-(1,10)phenanthroline, $H_2C_2O_4$ = oxalic acid), was hydrothermally synthesized and characterized by infrared spectrum, elemental analysis, single-crystal X-ray diffraction, power X-ray diffraction, and UV-vis absorption spectrum. Structural analyses reveal that polymer **1** possesses a (4, 4)-connected 2D network. In addition, **1** shows photocatalytic activity toward the degradation of rhodamine B (RhB) in the presence of H_2O_2 under visible light illumination.

Keywords: Fe-based coordination polymer, hydrothermal synthesis, crystal structure, photocatalytic activity; DOI: 10.14102/j.cnki.0254–5861.2011–2857

1 INTRODUCTION

The pollutants in wastewater have significant threat regarding humanity's daily life because they contain many kinds of refractory complex pollutant constituents, such as dye molecules, drugs, aromatic compounds, etc[1-3]. Especially, dye effluents are difficult to degrade. Even with quite low concentrations, they can still reduce the transmissivity of water and eventually destroy the ecosystems of water[4]. Thus, controlling the organic dye pollution in the water environment in time is urgent.

There are many conventional treatment methods to solve this problem, such as adsorption, microbial degradation, electrolysis, and so forth[5-7]. Among these ways, photocatalytic process has been recognized as one of the current technologies with energy-saving and high efficiency for the removal of pollutants from water[8]. Up to now, multitudinous inorganic materials have been adopted as photocatalysts for photocatalytic process[9-14]. Coordination polymers developed in recent years have been a new type of photocatalytic materials for their outstanding advantages of both organic and inorganic materials[15-17]. Coordination polymers are excellent composites combining high dimensional stability, rigidity of inorganic components as well as molecular decoration and clipping property of organic fractions, with more optimized functions[18-26]. In general, in order to obtain coordination polymers with desirable framework structures and functionalities, many efforts have been devoted to the rational selection of metal entities and organic linkers. In this regard, Fe-based polymers show great potential as photocatalysts, and have attracted extensive attention[27-29]. Meanwhile, owing to the rapid redox cycling of iron and faster production of ·OH, the Fe-based polymers were used as the catalyst and showed good catalytic effects. In addition, 1,10-phenanthroline (phen) and its derivatives with rigid planar and electron-poor heteroaromatic system are the ideal organic links to construct

Received 21 April 2020; accepted 28 June 2020 (**CCDC 1997930**)

① This project was supported by the National Natural Science Foundation of China (No. 21576112), the Project of Department of Science & Technology of Jilin Province (No. 20180623042TC), Natural Science Foundation Project of Jilin Province (No. 20170520143JH), the China Postdoctoral Science Foundation (No. 2017M611732), the Science and Technology Research Projects of the Education Department of Jilin Province (No. JJKH20180791KJ) and the Science and Technology Development Plan of Siping City (2017056)

② Corresponding authors. Li Chun-Xiang, professor, born in 1964, E-mail: lcx@ujs.edu.cn;
Che Guang-Bo, professor, born in 1973, E-mail: guangboche@jlnu.edu.cn

coordination polymers[30-36]. Many studies have shown that phen and its derivatives are good electron-transporting materials, and have a bright future, which will help the electrons and holes to separate, so the catalytic effects may be improved[37, 38].

Herein, we report a new Fe-based coordination polymer, $[Fe(C_2O_4)_{0.5}(4\text{-NCP})]_n \cdot nH_2O$ (**1**), with 1,10-phenanthroline derivative (2-(4-carboxyphenyl)-1H-imidazo(4,5-f)-(1,10)-phenanthroline, 4-HNCP) and oxalic acid ($H_2C_2O_4$) as the organic ligands and Fe(II) as the metal center. **1** was characterized by infrared spectrum, elemental analysis, single-crystal X-ray diffraction, power X-ray diffraction (XRD), and ultraviolet-visible (UV-vis) absorption spectrum. The photocatalytic activity toward the degradation of rhodamine B (RhB) dye was investigated from aqueous solution in the presence of H_2O_2 under visible light irradiation.

2 EXPERIMENTAL

2. 1 Chemicals

$FeSO_4 \cdot 7H_2O$ and oxalic acid ($H_2C_2O_4 \cdot 2H_2O$) were purchased from Sinopharm, China. 4-HNCP was purchased from Jinan Henghua Sci. & Tec. Co. Ltd, China. The other chemicals used in this study were of analytical grade without further purification.

2. 2 Preparation of 1

1 was prepared by hydrothermal process. $FeSO_4 \cdot 7H_2O$ (0.0278 g, 0.1 mmol), $H_2C_2O_4 \cdot 2H_2O$ (0.0126 g, 0.1 mmol) and 4-HNCP (0.017 g, 0.05 mmol) were added into 15 mL of aqueous solution. The mixture was stirred for 30 min at room temperature, and then transferred into a 25 mL Teflon-lined stainless-steel autoclave and heated at 443 K for 72 h. Upon cooling and opening the bomb, brown block crystals of **1** were collected with a yield of 45% (based on Fe) by filtration and washed with distilled water. Elemental anal. Calcd. (%) for $C_{21}H_{12}N_4O_6Fe$ (**1**, M_r = 472.20): C, 25.22; H, 12.10; N, 56.03. Found (%): C, 25.35; H, 12.21; N, 55.96. IR (cm^{-1}): 3414s, 1642s, 1588s, 1554s, 1449m, 1391s, 1311s, 1079m, 1014s, 967m, 922w, 794w, 730w, 532w, 492w.

2. 3 Characterization

Elemental analysis for C, H and N was carried out on a Perkin-Elmer 240C elemental analyzer. The infrared (IR) spectrum was recorded as KBr pellets on a Perkin-Elmer 2400LSII spectrometer. Powder X-ray diffraction (PXRD) patterns were characterized by D/MAX-3C diffractometer with Cu$K\alpha$ radiation (λ = 1.5406 Å). The morphology of **1** was observed by a JSM-6510 scanning electron microscope (SEM). The surface composition and chemical environment were analyzed by X-ray photoelectron spectroscopy (XPS, VG Scientific). Thermogravimetric analysis (TGA) of **1** was performed on a NETZSCH STA 449C analyzer heated from 40 to 1000 °C under N_2 atmosphere. The UV-vis spectra were recorded by Shimadzu UV-2500 spectrometer with $BaSO_4$ as reference.

2. 4 Single-crystal structure determination

Single-crystal X-ray diffraction data for polymer **1** were measured at 293(2) K on a Bruker SMART APEX CCD area detector diffractometer by graphite-monochromated Mo$K\alpha$ radiation (λ = 0.71073 Å). The structure was solved by direct methods of SHELXS-97 and refined by full-matrix least-squares techniques using the SHELXL-97 program[39, 40]. The non-hydrogen atoms were anisotropically refined against F^2 by the full-matrix least-squares technique. **1** crystallizes in triclinic system, space group $P\bar{1}$ with a = 8.5721(9), b = 9.3063(11), c = 12.3923(14) Å, α = 98.181(2)°, β = 92.118(2)°, γ = 110.166(2)°, V = 914.60(18) $Å^3$, Z = 2, $C_{21}H_{12}N_4O_6Fe$, M_r = 472.20, D_c = 1.715 g·cm^{-3}, μ = 0.877 mm^{-1}, F(000) = 480, *GOOF* = 1.032, the final R = 0.0468 and wR = 0.1017 for 2758 observed reflections with $I > 2\sigma(I)$. The selected bond distances of the title complex are given in Table 1.

Table 1. Selected Bond Length (Å) and Bond Angle (°) for 1

Bond	Dist.	Bond	Dist.	Bond	Dist.
Fe(1)–N(1)	2.185(3)	Fe(1)–N(2)	2.176(3)	Fe(1)–O(2)	2.131(2)
Fe(1)–O(1)	2.161(2)	Fe(1)–O(4)	2.026(2)	Fe(1)–O(3)	2.196(2)
Angle	(°)	Angle	(°)	Angle	(°)
O(4)–Fe(1)–O(2)	92.97(10)	O(4)–Fe(1)–O(1)	97.99(10)	O(2)–Fe(1)–O(1)	90.84(9)
O(4)–Fe(1)–N(2)	94.75(10)	O(2)–Fe(1)–N(2)	171.67(10)	O(1)–Fe(1)–N(2)	91.17(9)
O(4)–Fe(1)–N(1)	167.71(11)	O(2)–Fe(1)–N(1)	96.44(10)	O(1)–Fe(1)–N(1)	89.77(10)
N(2)–Fe(1)–N(1)	75.49(10)	O(4)–Fe(1)–O(3)	88.90(10)	O(2)–Fe(1)–O(3)	76.77(9)
O(1)–Fe(1)–O(3)	166.16(9)	N(2)–Fe(1)–O(3)	100.24(9)	N(1)–Fe(1)–O(3)	85.59(10)

2. 5 Photocatalytic test

In a typical photocatalytic degradation process, 20 mg of **1** was mixed with an aqueous solution of RhB (100 mL, 10 mg/L) in a glass reaction flask. After the dark adsorption in 30 min, H_2O_2 (2 mmol) was added to the mixture solution. Afterwards, the suspension was exposed to visible-light illumination using a 250W Xe lamp with a cut off filter (420 nm). At every 20 min interval, 4 mL of the suspension was extracted and RhB solution was measured using a UV-vis spectrophotometer after centrifugation.

3 RESULTS AND DISCUSSION

3. 1 Crystal structure of 1

The single-crystal X-ray crystallographic study reveals that **1** crystallizes in the triclinic crystal system with $P\bar{1}$ space group. The crystal structure of **1** possesses a 2D network with one Fe(II) center, one 4-NCP ligand, a half C_2O_4 anion and two free water molecules in the asymmetric unit. Each Fe(II) center is six-coordinated [FeO_4N_2] in an octahedral coordination environment (Fig. 1). The basal plane and apical positions are occupied by N(1), N(2), O(2), O(4) and O(1), O(3), respectively. The Fe–O bond lengths are in the range of 2.026(2)～2.196(2) Å and the Fe–N bond lengths are 2.185(3) and 2.176(3) Å (Table 1), which are in accord with those reported Fe(II) complexes[41]. It is more interesting that adjacent four Fe(II) centers are connected by 4-NCP ligands in (κ^1-κ^1)-(κ^1-κ^1)-μ_3 modes, leading to a novel 1-D double chain structure, with the Fe⋯Fe distances of 4.7134 and 15.3265 Å (Fig. 2). There exist π-π interactions between the neighboring 4-NCP ligands in the 1D chains, as indicated by a center-to-center distance of 3.523(2) Å, a dihedral angle of 6.85(17)°. In addition, these 1D chains are connected with each other through C_2O_4 ligands in (κ^1-κ^1)-(κ^1-κ^1)-μ_2 manners, resulting in a 2D network, with the Fe⋯Fe distances of 5.5935 and 15.3265 Å. The overall network topology of **1** can be described as a (4,4)-connected network. In addition, hydrogen bonds of O–H⋯O interactions are also found in the 2D network between the coordinated water molecules and carboxylic oxygen atoms, which further stabilize the 2D network (Table 2).

Table 2. Hydrogen-bonding Geometry (Å, °) for 1

D–H⋯A	d(D–H)	d(H⋯A)	d(D⋯A)	∠DHA
O(1W)–H(1WA)⋯O(3)$^{\#3}$	0.76	2.03	2.776(4)	167
O(1W)–H(1WB)⋯O(2W)	0.87	1.94	2.798(5)	166

Symmetry code for **1**: #3: *x*+1, *y*, *z*

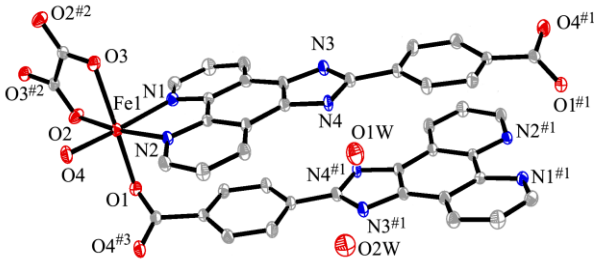

Fig. 1. Coordination environment of Fe atom in 1. Symmetry codes: #1: 1–*x*, 1–*y*, 1–*z*; #2: 2–*x*, –*y*, –*z*; #3: 2–*x*, 1–*y*, –*z*

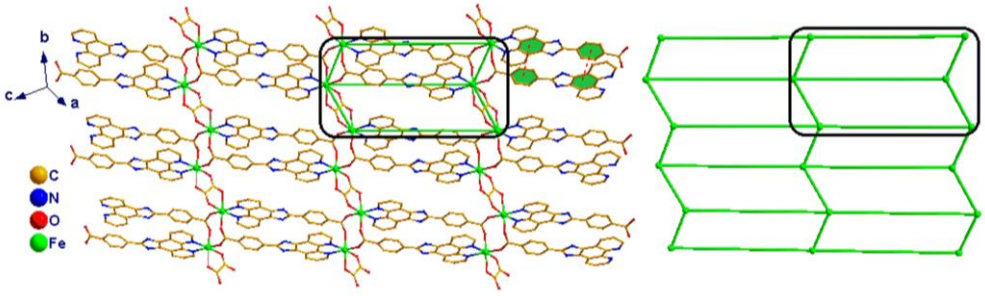

Fig. 2. View of the 2D structure of 1 (left) and (4,4) net topology of the 2D layer (right)

3. 2 Characterization of 1

The morphology and particle size of **1** were examined by SEM (Fig. 3). The as-prepared **1** sample is composed of block-like crystal with a length of tens of micrometers. The experimental and computer-simulated powder X-ray diffraction (XRD) patterns of **1** are presented in Fig. 4. They coincided well between the as-synthesized pattern and the simulated one, which indicates the phase purities of the sample. Fig. 5 shows XPS spectra of Fe orbitals before and after photocatalytic process. The consistency of XPS spectra before and after the catalysis indicated that the structure of **1** is intact and not collapse.

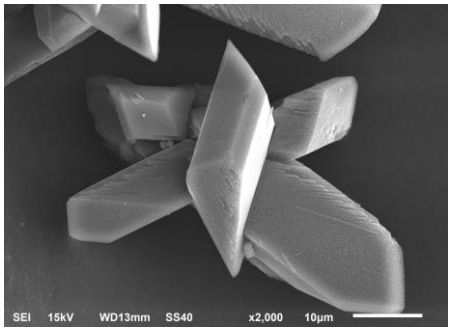

Fig. 3. SEM image of 1

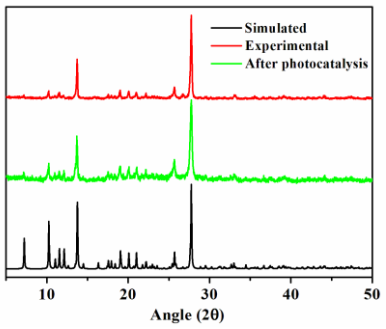

Fig. 4. PXRD patterns of the simulated (black), as-synthesized 1 (red), and after photocatalysis RhB (green)

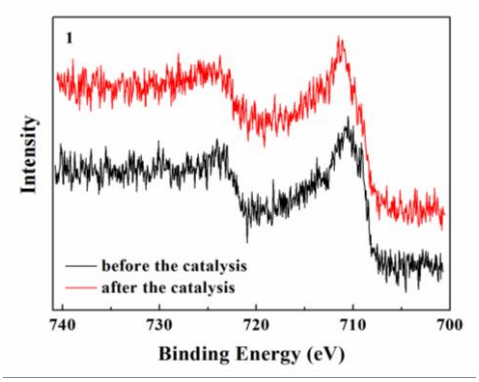

Fig. 5. XPS spectra of Fe orbital of 1 before and after catalysis

The UV-Vis diffuse reflectance spectrum is recorded to estimate the UV-vis absorption spectrum of **1**. As shown in Fig. 6, **1** displays strong absorption in the range of 200～750 nm, which can be attributed to absorption induced by ligand-to-metal charge transfer (LMCT). The absorption onset of **1** is located at approximately 486 nm; thus, based on the relation $E_g = 1240/\lambda$[42], the calculated bandgap of **1** is 2.55 eV (inset in Fig. 6).

The thermal behavior of **1** was studied by TGA. As shown in Fig. 7, the TG curve of **1** shows two main steps of weight loss in the temperature range of 40～1000 °C. The weight loss of 7.45% from 60 to 133 °C results from the release of water molecules (calcd. 7.62%), and that from 231 °C corresponds to the decomposition and collapse of the structure.

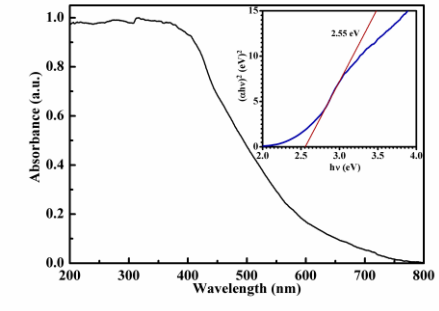

Fig. 6. UV-Vis diffuse reflectance spectrum of 1

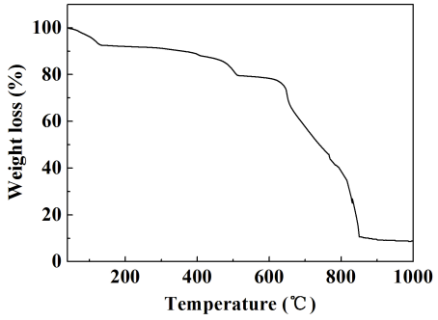

Fig. 7. TGA curve of polymer 1

3. 3 Catalytic activity of 1

The photodegradation of RhB was carried out under irradiation by visible light to evaluate the catalytic performance of **1**. Fig. 8a displays the variations of RhB concentration (C/C_0) as a function of reaction time under different conditions. After visible light irradiation for 80 min, no observation of the photolysis of RhB in the absence of the catalyst **1**, reflecting that RhB was quite stable toward incident light. As shown in Fig. 8a, only 4.68% of RhB was degraded in 80 min with the addition of H_2O_2 under visible light irradiation. And when only catalyst **1** was added under visible light irradiation, 4.93% of RhB was removed within 80 min. On the other hand, 25.16% of RhB was degraded in the presence of **1** and H_2O_2 under dark condition. Interestingly, 99.50% of RhB was decomposed after 80 min, when using **1** with H_2O_2 irradiated by visible light. As shown in Fig. 8b, the visible band of the dye decreased gradually as the reaction progressed. The photocatalytic activity of bare **1** was not satisfactory due to the rapid recombination of photogenerated electron-hole pairs according to the literature[27-29]. Intriguingly, the introduction of external H_2O_2 could hinder the recombination of photogenerated carriers and improve the photocatalytic activity of **1**. The results demonstrate **1** exhibits good photocatalytic activity for RhB degradation in the presence of H_2O_2 under visible irradiation.

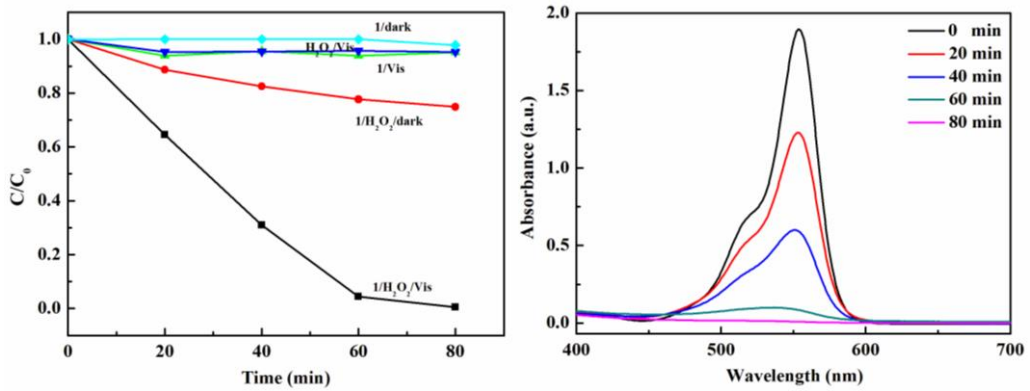

Fig. 8. (a) Degradation of RhB under different reaction conditions. (b) UV-vis spectral changes during RhB decolorization by 1

To determine the catalytic mechanism of **1**, trapping experiments of active species were performed. The isopropanol (IPA), ammonium oxalate (AO) and benzoquinone (BQ) were applied to the reaction system as · OH, h^+ and · O_2^- scavengers, respectively. As shown in Fig. 9, in the presence of IPA, AO and BQ, the degradation efficiencies of RhB were 13.08%, 20.79% and 61.77%, respectively. The inhibitory effects of IPA and AO were much higher under visible light irradiation, contrast to the BQ scavenger. The free radical trapping experiments indicated that · OH and h^+ are the major active species during the photocatalytic process. Fig. 10 shows the measured photocatalytic stability of **1**. The photocatalytic efficiency decreased slightly through each cycle, indicating good reusability of **1** for RhB degradation under visible-light irradiation.

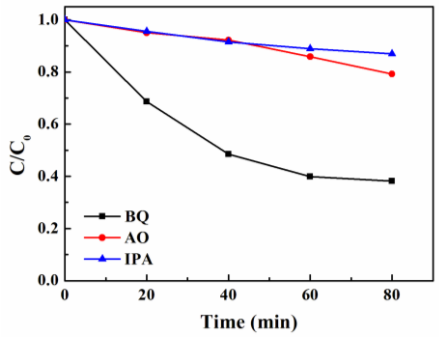

Fig. 9. Trapping experiments of active species during the photocatalytic reaction

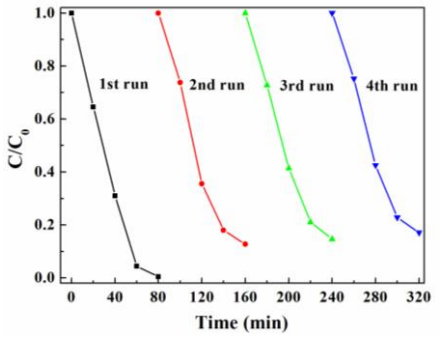

Fig. 10. Reusability of 1 for the photocatalytic degradation of RhB under visible-light irradiation

4 CONCLUSION

A novel Fe-based coordination polymer was synthesized based on 4-HNCP and $H_2C_2O_4$ ligands under hydrothermal conditions. Polymer **1** possesses a (4,4)-connected 2D network and further stabilizes the 2D framework through hydrogen bonding O–H ··O interactions. Besides, polymer **1** exhibits good photocatalytic activity for RhB degradation in the presence of H_2O_2 under visible irradiation. 99.50% of RhB was degraded after 80 min in the presence of **1** and H_2O_2, which reveals **1** has promise as a photocatalyst for the treatment of dye wastewater.

REFERENCES

(1) Zangeneh, H.; Zinatizadeh, A, A, L.; Habibi, M.; Akia, M.; Isa, M. H. Photocatalytic oxidation of organic dyes and pollutants in wastewater using different modified titanium dioxides: a comparative review. *J. Ind. Eng. Chem*. **2015**, 26, 1–36.

(2) Rosal, R.; Rodr guez, A.; Perdig nmel n, J. A.; Petre, A.; Garc acalvo, E.; G mez, M. J.; Ag era, A.; Fern ndez-Alba, A. R. Occurrence of emerging pollutants in urban wastewater and their removal through biological treatment followed by ozonation. *Water Res*. **2010**, 44, 578–588.

(3) Deblonde, T.; Cossuleguille, C.; Hartemann, P. Emerging pollutants in wastewater: a review of the literature. *Int. J. Hyg. Envir. Heal*. **2011**, 214, 442–448.

(4) Banat, I. M.; Nigam, P.; Singh, D.; Marchant, R. Microbial dye reduction of textile-dye-containing effluents: a review. *Bioresource Technol*. **1996**, 58, 217 coordination polymers 227.

(5) Yu, Y.; Yu, J. C.; Chan, C. Y.; Che, Y. K.; Zhao, J. C.; Ding, L. Ge, W. K.; Wong, P. K. Enhancement of adsorption and photocatalytic activity of TiO_2 by using carbon nanotubes for the treatment of azo dye. *Appl. Catal. B: Environ*. **2005**, 61, 1–11.

(6) McMullan, G.; Meehan, C.; Conneely, A.; Kirby, N.; Robinson, T.; Nigam, P.; Banat, I.; Marchant, R.; Smyth, W. Microbial decolourisation and degradation of textile dyes. *Appl. Microbiol. Biot*. **2001**, 56, 81–87.

(7) Qin, L.; Zhang, G.; Meng, Q.; Xu, L.; Lv, B. Enhanced MBR by internal micro-electrolysis for degradation of anthraquinone dye wastewater. *Chem. Eng. J*. **2012**, 210, 575–584.

(8) Mills, A.; Hunte, S. L. An overview of semiconductor photocatalysis. *J. Photochem. Photobiol. A* **1997**, 10, 1–35.

(9) Kalan, R. E.; Yaparatne, S.; Amirbahman, A.; Tripp, C. P. P25 titanium dioxide coated magnetic particles: Preparation, characterization and photocatalytic activity. *Appl. Catal. B: Environ*. **2016**, 187, 249–258.

(10) Tang, A. M.; Hu, T. T.; Su, X. Fabrication of microcrystalline cellulose/CdS nanocomposites and their photocatalytic properties. *Adv. Mater. Res*. **2013**, 638, 2475–2480.

(11) Pei, Z. X.; Ding, L. Y.; Lu, M. L.; Fan, Z. H.; Weng, S. X.; Hu, J.; Liu, P. Synergistic effect in polyaniline-hybrid defective ZnO with enhanced photocatalytic activity and stability. *J. Phys. Chem. C* **2014**, 118, 9570–9577.

(12) W. L.; Shi, C.; Liu, M. Y.; Li, X.; Lin, F.; Guo, J. Y.; Shi, Fabrication of ternary $Ag_3PO_4/Co_3(PO_4)_2/g\text{-}C_3N_4$ heterostructure with following Type II and Z-Scheme dual pathways for enhanced visible-light photocatalytic activity, *J. Hazard. Mater*. **2020**, 389, 121907.

(13) Yang, S.; Liu, C.; Wang, J. B.; Lin, X; Hong, Y. Z.; Guo, F.; Shi, J. Y. Enhanced photocatalytic activity of $g\text{-}C_3N_4$ quantum dots/$Bi_{3.64}Mo_{0.36}O_{6.55}$ nanospheres composites. *J. Solid State Chem*. **2020**, 287, 121347.

(14) Wang, J. B.; Liu, C.; Yang, S.; Lin, X.; Shi, W. L. Fabrication of a ternary heterostructure $BiVO_4$ quantum dots/$C_{60}/g\text{-}C_3N_4$ photocatalyst with enhanced photocatalytic activity. *J. Phys. Chem. Solids* **2020**, 136, 109164.

(15) Dai, M.; Li, H. X.; J. Lang, P. New approaches to the degradation of organic dyes, and nitro- and chloroaromatics using coordination polymers as photocatalysts. *CrystEngComm*. **2015**, 17, 4741–4753.

(16) Wang, F.; Li, F. L.; Xu, M. M.; Yu, H.; Zhang, J. G.; Xia, H. T.; Lang, J. P. Facile synthesis of a Ag(I)-doped coordination polymer with enhanced catalytic performance in the photodegradation of azo dyes in water. *J. Mater. Chem. A* **2015**, 3, 5908–5916.

(17) Liu, C. Y.; Xu, L. Y.; Ren, Z. G.; Wang, H. F.; Lang, J. P. Assembly of silver(I)/N,N-bis(diphenylphosphanylmethyl)-3-aminopyridine/ halide or pseudohalide complexes for efficient photocatalytic degradation of organic dyes in water. *Cryst. Growth Des*. **2017**, 17, 4826–4834.

(18) Wang, M. F.; Mi, Y.; Hu, F. L.; Niu, Z.; Yin, X. H.; Huang, Q.; Wang, H. F.; Lang, J. P. Coordination-driven stereospecific control strategy for pure cycloisomers in solid-state diene photocycloaddition. *J. Am. Chem. Soc*. **2020**, 142, 700–704.

(19) Shi, Y. X.; Chen, H. H.; Li, W. X.; Zhang, W. H.; Day, G. S.; Lang, J. P.; Zhou, H. C. Photo-induced nonlinear negative expansion behavior in metal−organic frameworks. *Chem. Eur. J*. **2019**, 25, 8543–8549.

(20) Shi, Y. X.; Zhang, W. H.; Abrahams, B. F.; Braunstein, P.; Lang, J. P. Fabrication of new photoactuators: macroscopic photomechanical responses of

metal-organic frameworks to irradiation by UV light. *Angew. Chem., Int. Ed.* **2019**, 58, 9453–9458.

(21) Liu, G. C.; Li, Y.; Chi, J.; Xu, N.; Wang, X. L.; Lin, H. Y.; Chen, Y. Q. Multi-functional fluorescent responses of cobalt complexes derived from functionalized amide-bridged ligand. *Dyes and Pigments* **2020**, 174, 108064.

(22) Lee, J. Y.; Farha, O. K.; Roberts, J.; Scheidt, K. A.; Nguyen, S. T.; Hupp, J. T. Metal-organic framework materials as catalysts. *Chem. Soc. Rev.* **2009**, 38, 1450–1459.

(23) Zhang, W.; Xiong, R. G. Ferroelectric metal-organic frameworks. *Chem. Rev.* **2012**, 112, 1163–1195.

(24) Meek, S. T.; Greathouse, J. A.; Allendorf, M. D. Metal-organic frameworks: a rapidly growing class of versatile nanoporous materials. *Adv. Mater.* **2011**, 23, 249–267.

(25) Ge, J. Y.; Chen, Z. Y.; Zhang, L.; Liang, X.; Su, J.; Kurmoo, M.; Zuo, J. L. A two-dimensional iron(II) coordination polymer with synergetic spin-crossover and luminescent properties. *Angew. Chem. Int. Edit.* **2019**, 58, 8789–8793.

(26) Yaghi, O. M.; Li, G. M.; Li, H. L. Selective binding and removal of guests in a microporous metal-organic framework. *Nature* **1995**, 378, 703–706.

(27) Ai, L. H.; Zhang, C. H.; Li, L. L.; Jiang, J. Iron terephthalate metal-organic framework: revealing the effective activation of hydrogen peroxide for the degradation of organic dye under visible light irradiation. *Appl. Catal. B-Environ.* **2014**, 148–149, 191–200.

(28) Gao, Y. W.; Li, S. M.; Li, Y. X.; Yao, L. Y,; Zhang, H. Accelerated photocatalytic degradation of organic pollutant over metal-organic framework MIL-53(Fe) under visible LED light mediated by persulfate. *Appl. Catal. B-Environ.* **2017**, 202, 165–174.

(29) Xia, Q.; Wang, H.; Huang, B. B.; Yuan, X. Z.; Zhang, J. J.; Zhang, J.; Jiang, L. B.; Xiong, T.; Zeng, G. M. State-of-the-art advances and challenges of iron-based metal organic frameworks from attractive features, synthesis to multifunctional applications. *Small* **2018**, 1803088–25.

(30) Wang, X. L.; Chen, Y. Q.; Gao, Q.; Lin, H. Y.; Liu, G. C.; Zhang, J. X.; Tian, A. X. Coordination behavior of 5,6-substituted 1,10-phenanthroline derivatives and structural diversities by coligands in the construction of lead(II) complexes. *Cryst. Growth Des.* **2010**, 10, 2174–2184.

(31) Li, Z. M.; Qiao, Y.; Liu, C. B.; Zhou, Y. F.; Wang, X. Y.; Charpentier, P. A.; Che, G. B.; Xu, W. Z.; Liu, L. H.; Zhu, E. W. Syntheses, crystal structures, adsorption properties and visible photocatalytic activities of highly stable Pb-based coordination polymers constructed by 2-(2-carboxyphenyl)imidazo(4,5-f)-(1,10)phenanthroline and bridging linkers. *Dalton Trans*. **2018**, 47, 7761–7775.

(32) Li, X. Y.; Yin, T. Q.; Wang, C. Y.; Zhang, J.; Wang, Y.; Gao, L.; Hu, B.; Liu, B.; Jiang, W.; Che, G. B. Synthesis, crystal structure and theoretical calculation of a novel 2D network of manganese(II) complex. *Chin. J. Struct. Chem.* **2019**, 38, 2113–2120.

(33) Wei, Y. Q.; Yu, Y. F.; Wu, K. C. Highly stable diamondoid network coordination polymer $[Mn(NCP)_2]_n$ with notable NLO, magnetic, and luminescence properties. *Cryst. Growth Des.* **2007**, 7, 2262–2264.

(34) Li, X. Y.; Liu, C. B.; Che, G. B.; Wang, X. C.; Li, C. X.; Yan, Y. S.; Guan, Q. F. Four metal-organic networks based on benzene-1,4-dioxyacetic acid and dipyrido[3,2-a:2′,3′-c]phenazine ligand. *Inorg. Chim. Acta* **2010**, 363, 1359–1366.

(35) Kong, Z. G.; Han, Q.; Zhang, L.; Liu, D. X.; Hu, B.; Wang, X. Y. A new Cd(II) coordination polymer constructed by 1,10-phenanthroline derivative: Syntheses, structure, physical properties and theoretical calculation. *Chin. J. Struct. Chem.* **2019**, 38, 2141–2147.

(36) Wang, X. Y.; Li, X. M.; Pan, Y. R.; Liu, B.; Zhou, S. A new two-dimensional Cd(II) complex assembled by 1,3,5-benzenetricarboxylic acid and 3-(2-pyridyl)pyrazole. *Chin. J. Struct. Chem*. **2019**, 38, 1275–1282.

(37) Li, Y. Q.; Fung, M. K.; Xie, Z. Y.; Lee, S. T.; Hung, L. S.; Shi, J. M. An efficient pure blue organic light-emitting device with low driving voltages. *Adv. Mater*. **2002**, 14, 1317–1321.

(38) Jang, J. G.; Ji, H. J.; Kim, H. S.; Jeong, J. C. TPBI: FIrpic organic light emitting devices with the electron transport layer of Bphen/Alq_3. *Curr. Appl. Phys*. **2011** , 11, S251–S254.

(39) Sheldrick, G. M. *SHELXS-97, Programs for X-ray Crystal Structure Solution*. University of Göttingen, Germany **1997**.

(40) Sheldrick, G. M. *SHELXL-97, Programs for X-ray Crystal Structure Refinement.* University of Göttingen, Germany **1997**.

(41) Wang,X. L.; Yang, P. P.; Li, Z. W.; Li, L. C.; Liao, D. Z. Syntheses, structures, and magnetic properties of three Fe(II) complexes with reduced radical ligands. *Inorg. Chim. Acta*. **2009**, 362, 1901–1906.

(42) Long, J. L.; Wang, S. B. ; Ding, Z. X.; Wang, S. C.; Zhou, Y. G.; Huang, L.; Wang, X. X. Amine-functionalized zirconium metal–organic framework as efficient visible-light photocatalyst for aerobic organic transformations. *Chem. Commun*. **2012**, 48, 11656–11658.